Translational Stroke Research
https://doi.org/10.1007/s12975-024-01273-6

RESEARCH

Complement Inhibition Reduces Early Erythrolysis, Attenuates Brain Injury, Hydrocephalus, and Iron Accumulation after Intraventricular Hemorrhage in Aged Rats

Tianjie Zhang[1,2] · Fan Xia[1,2] · Yingfeng Wan[1] · Guohua Xi[1] · Hua Ya[1] · Richard F. Keep[1]

Received: 22 March 2024 / Revised: 3 June 2024 / Accepted: 20 June 2024

Abstract

Blood components released by erythrolysis play an important role in secondary brain injury and posthemorrhagic hydrocephalus (PHH) after intraventricular hemorrhage (IVH). The current study examined the impact of N-acetylheparin (NAH), a complement inhibitor, on early erythrolysis, PHH and iron accumulation in aged rats following IVH. This study, on 18-months-old male Fischer 344 rats, was in 3 parts. First, rats had an intracerebroventricular injection of autologous blood (IVH) mixed with NAH or saline, or saline alone. After MRI at four hours, Western blot and immunohistochemistry examined complement activation and electron microscopy choroid plexus and periventricular damage. Second, rats had an IVH with NAH or vehicle, or saline. Rats underwent serial MRI at 4 h and 1 day to assess ventricular volume and erythrolysis. Immunohistochemistry and H&E staining examined secondary brain injury. Third, rats had an IVH with NAH or vehicle. Serial MRIs on day 1 and 28 assessed ventricular volume and iron accumulation. H&E staining and immunofluorescence evaluated choroid plexus phagocytes. Complement activation was found 4 h after IVH, and co-injection of NAH inhibited that activation. NAH administration attenuated erythrolysis, reduced ventricular volume, alleviated periventricular and choroid plexus injury at 4 h and 1 day after IVH. NAH decreased iron accumulation, the number of choroid plexus phagocytes, and attenuated hydrocephalus at 28 days after IVH. Inhibiting complement can reduce early erythrolysis, attenuates hydrocephalus and iron accumulation after IVH in aged animals.

Keywords Intraventricular hemorrhage · Erythrolysis · Hydrocephalus · Iron accumulation · Complement · N-acetylheparin · NAH

Introduction

Intraventricular hemorrhage (IVH) has high mortality and poor prognosis in both adult and neonatal patients. In adults, IVH independently serves as a predictor of poor prognosis among intracerebral hemorrhage (ICH) patients [1, 2]. In addition, up to 50% of patients with IVH secondary to ICH develop post-hemorrhagic hydrocephalus (PHH), which is also associated with worse neurological outcomes [3]. IVH following germinal matrix hemorrhage (GMH) also occurs in approximately 25–30% of preterm infants, and 8–10% of GMH/IVH infants will develop PHH [4].

The etiology of PHH is still not fully clear, and treatment options are limited. Intraventricular injection of recombinant tissue plasminogen activator (rt-PA) to speed clot clearance reduced mortality in adult IVH patients but it did not significantly improve the long-term neurological outcomes [5]. For hydrocephalus, the only effective treatment is surgical, with temporary external cerebrospinal fluid (CSF) drainage, a permanent shunt or third ventriculostomy [6]. Unfortunately, these treatments are associated with about 40% reoperation rates [7, 8]. It not only increases the risk of intracranial infection in patients [9, 10], but also brings long-term heavy psychological burden [11]. Therefore, IVH and PHH urgently need new potential therapeutic targets.

Multiple studies have shown that the release of hemoglobin and iron after red blood cell lysis causes intense

Tianjie Zhang and Fan Xia contributed equally to this work.

✉ Richard F. Keep
rkeep@umich.edu

[1] Department of Neurosurgery, University of Michigan, R5018 BSRB 109 Zina Pitcher Place, Ann Arbor, MI 48109, USA

[2] Department of Neurosurgery, West China Hospital, Sichuan University, Chengdu, China

Published online: 28 June 2024

inflammation after IVH, contributing to severe secondary brain injury and PHH [12–15]. The activation of complement system plays a crucial role in erythrolysis. Our prior studies found rapid complement system activation after ICH leading to membrane attack complex (MAC) formation which mediates erythrolysis [16–18]. However, early complement cascade activation have been insufficiently studied in IVH.

In two recent studies, complement inhibition effectively attenuated ventricular dilatation after collagenase-induced neonatal GMH/IVH [19, 20]. Our prior study demonstrated that MAC inhibition can decrease ventricular volume and iron deposition in both acute and chronic phase of IVH in young adult rats [21]. These studies indicate that complement inhibition is a promising therapeutic target to alleviate secondary brain injury and PHH after IVH. However, these preclinical studies used only neonatal and young adult rodents. ICH and subsequent IVH is mostly a disease of the elderly. Considering inflammation and PHH are also more severe in aged than in young rats [22], it is necessary to verify the effect of complement inhibition in aged rodents.

N-acetylheparin (NAH) is an inhibitor of complement activation. Previous studies have indicated that NAH exhibits protective effects on heart, lung, and brain tissue by inhibiting complement activation [23–25]. Our prior study found that co-injection of NAH attenuated erythrolysis induced secondary brain injury and iron accumulation in aged rats after ICH [26]. However, the effect of NAH in IVH remains unclear. The goals of this study were, therefore, to examine the effects of NAH in aged rats with IVH, including effects on erythrolysis, hydrocephalus, secondary brain injury and iron deposition.

Methods

Animal Preparation and Intraventricular Injection

Animal procedures were approved by the University of Michigan Committee on Use and Care of Animals. The study complies with ARRIVE guidelines for reporting in vivo animal experiments [27]. A total of 76 male 18-month-old Fischer 344 rats (National Institutes of Health, Bethesda, MD) were used. Experimental animals were allocated using odd/even numbers to ensure randomization. Rats were housed in a 12-h light/12-h dark cycle environment and provided with ad libitum access to food and water.

For establishing the IVH model, rats underwent anesthesia with 50 mg/kg pentobarbital intraperitoneally, and their rectal temperature was sustained at 37 °C by a feedback-controlled heating pad. The right femoral artery was catheterized for autologous blood collection. After placement in a stereotactic frame, a midline scalp incision (~5 mm) was made. Then a cranial burr hole was drilled, and autologous blood, with NAH or vehicle, or saline, was administered with a 26-gauage needle into the right lateral ventricle (0.6 mm posterior, 1.6 mm lateral, 4.5 mm ventral to the bregma) at a rate of 14 µl/min [22]. The needle was left in place for a further 5 min before withdrawal. The drilled hole was sealed using bone wax and the incision sutured.

Experimental Groups

The study was divided into three parts. In the first, rats received an intracerebroventricular (icv) injection of either: 1) 200µL autologous blood with 5µL saline (IVH + Vehicle), 2) 200µL autologous blood with 20 µg/5µL NAH/saline (IVH + NAH), or 3) 205µL saline (IVS). The chosen concentration of NAH was based on previous findings demonstrating its efficacy in reducing brain injury and erythrolysis in a rat ICH model [26]. Rats underwent MRI examination at 4 h after injection and were subsequently euthanized. Brains were used for Western blot analysis ($n = 4$ each group) and electron microscopy ($n = 2$ in IVH + Vehicle/NAH group). In the second part, rats received: 1) 200µL autologous blood with 5µL saline, 2) 200µL autologous blood with 20 µg/5µL NAH/saline, or 3) 205µL saline. Rats underwent serial MRI scans at 4 h and 1 day. Euthanasia was performed at day 1, and the brains used for histology ($n = 8$ each group). In the third part, rats were administered either 200µL autologous blood with 5µL saline or 20 µg/5µL NAH/saline. Serial MRI scans were performed on days 1 and 28. Rats were euthanized on day 28 for brain histology ($n = 8$ each group). Another 10 naïve aged rats underwent MRI to serve as controls.

Following intraventricular injection, the mortality rates were as follows: IVH + Vehicle group (6/28), IVH + NAH (3/25), and IVS group (1/13). All deceased animals were removed from further analysis.

Magnetic Resonance Imaging

Rats were anesthetized with isoflurane (2%) in a 7.0-T MR scanner (Bruker Inc.). T2-weighted fast spin-echo (TR/TE = 4000/60 ms) as well as T2*-weighted gradient-echo sequences (TR/TE = 4000/60 ms) were acquired at various time points after injection. The field of view was 35 × 35 mm and the matrix was 256 × 128 mm. Every sequence consisted of 25 coronal slices (0.5 mm thick), covering the whole lateral ventricles. Bilateral ventricular volumes were calculated following established procedures [14]. Briefly, ventricle volume was determined by multiplying the sum of ventricular area of each layer by slice thickness.

The intraventricular T2* lesion indicates hematoma during the acute phase (4 h and 1d) and iron accumulation

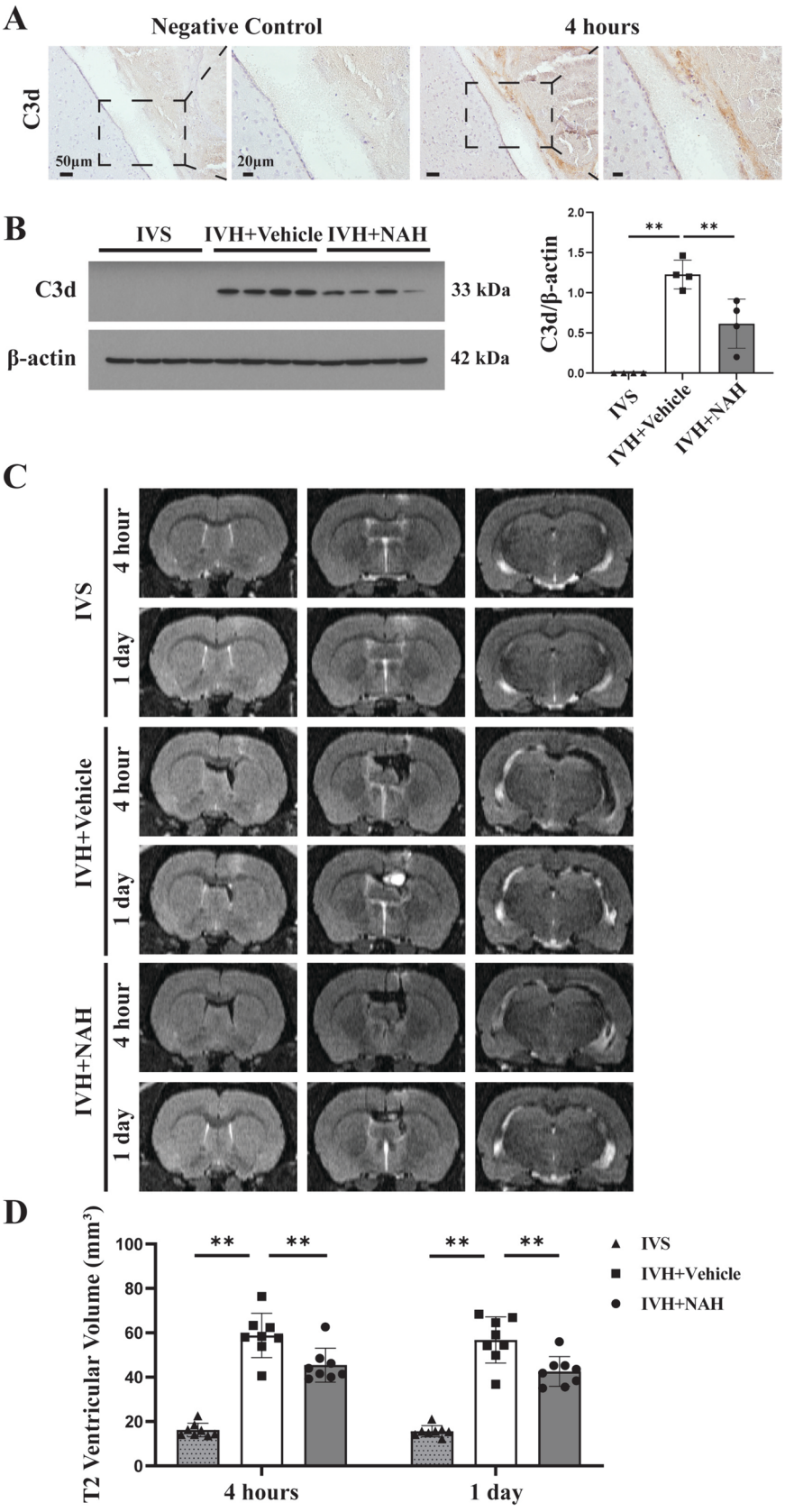

Fig. 1 NAH administration reduced complement activation and ventricular dilation in the acute phase after IVH. **A** Immunohistochemistry staining for C3d in F344 aged rats 4 h after IVH. C3d positive cells could be seen within the hematoma, which is not seen in negative controls. Left panels scale bars are 50μm and right panels scale bars are 20μm. **B** Western blot analysis of complement C3d protein levels in periventricular area 4 h after intraventricular injection of blood and NAH (IVH + NAH) or blood and saline (IVH + Vehicle), or saline (IVS) in aged rats (β-actin served as a loading control). C3d protein levels were quantified (bar graph). Values are means ± SD, $n = 4$ per group, $^{*}p < 0.01$. **C** Representative coronal T2-weighted MRI scans at 4 h and 1 day in the IVH + NAH, ICH + Vehicle and IVS groups. **D** Ventricular volumes quantification. Data are means ± SD, $n = 8$ per group. There was significant ventricular dilation after IVH compared to IVS controls. NAH rats had significantly smaller ventricular volumes than vehicle treated rats at both 4 h and 1 day after IVH. $^{**}p < 0.01$

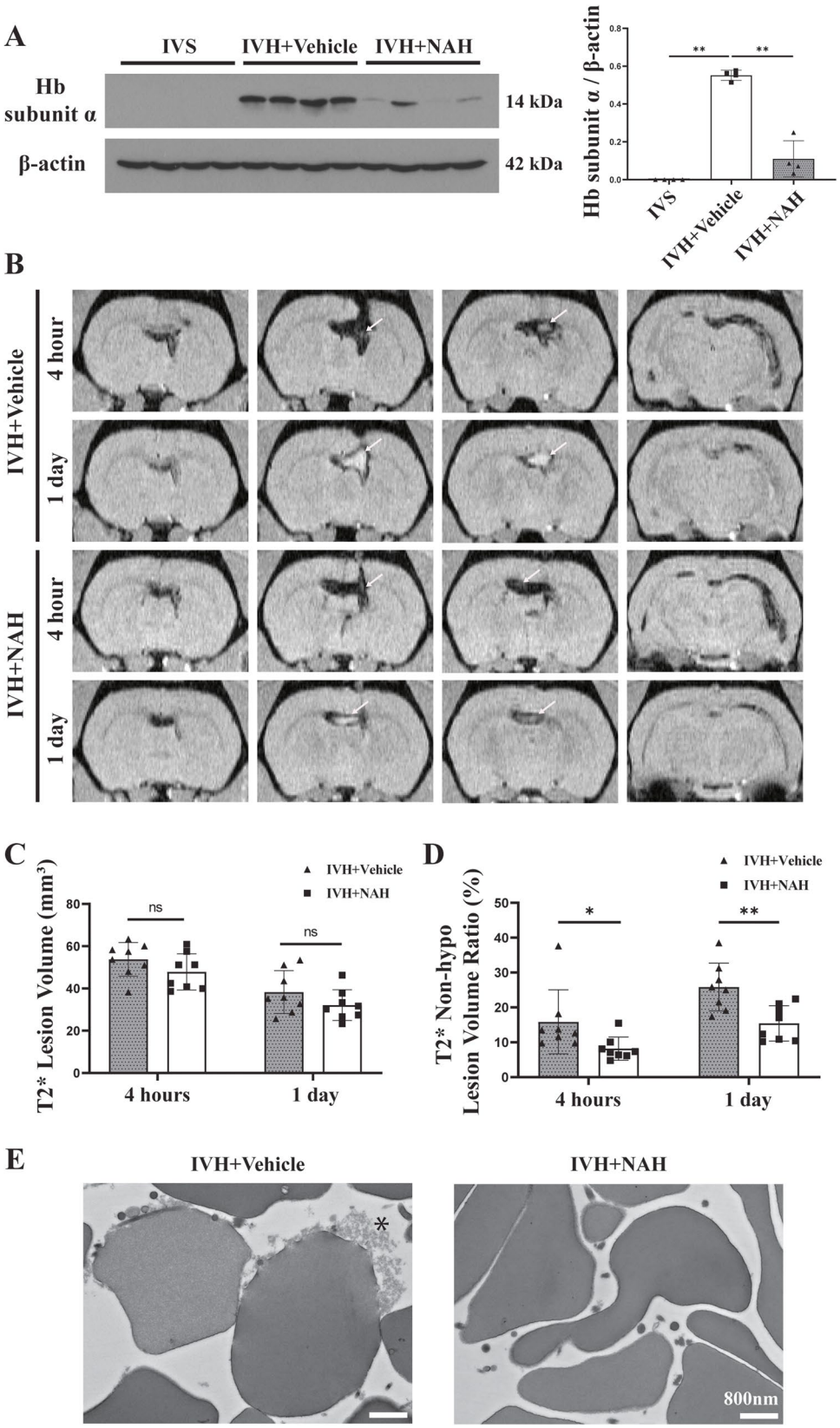

Fig. 2 NAH attenuated erythrolysis without significantly affecting hematoma volume after IVH. **A** Western blot analysis of hemoglobin subunit α protein levels in periventricular area at 4 h after intraventricular injection of blood and NAH (IVH + NAH), blood and saline (IVH + Vehicle), or saline (IVS) in aged rats (β-actin acted as loading control). Hb subunit α levels were quantified (bar graph). Values are means ± SD, $n = 4$ per group, $^{**}p < 0.01$. **B** Representative T2*-weighted MRIs at 4 h and 1 day in IVH + NAH and IVH + vehicle groups. Hypointense hematoma and non-hypointense lesion (white arrows) can be noted on T2* sequence. **C** T2*-weighted hematoma volumes at 4 h and 1-day post-surgery. There were no significant differences (ns) in hematoma volume between NAH and vehicle groups at either time point. **D** Intraventricular non-hypointense lesion volumes (as a % of total T2* lesion volume) at 4 h and 1 day after IVH to assess erythrolysis. The NAH group had a lower T2* non-hypointense lesion volume ratio than vehicle-treated rats at both time points. Values are means ± SD; $n = 8$ per group, $^{*}p < 0.05$, $^{**}p < 0.01$. **E** Representative electron microscopy images of erythrocytes after 4 h in the IVH + NAH and IVH + vehicle group. Note the evidence of erythrolysis in the IVH + vehicle group with loss of intracellular content to the extracellular space (*). In contrast, in the IVH + NAH group, erythrocytes show intact membranes, $n = 2$ per group

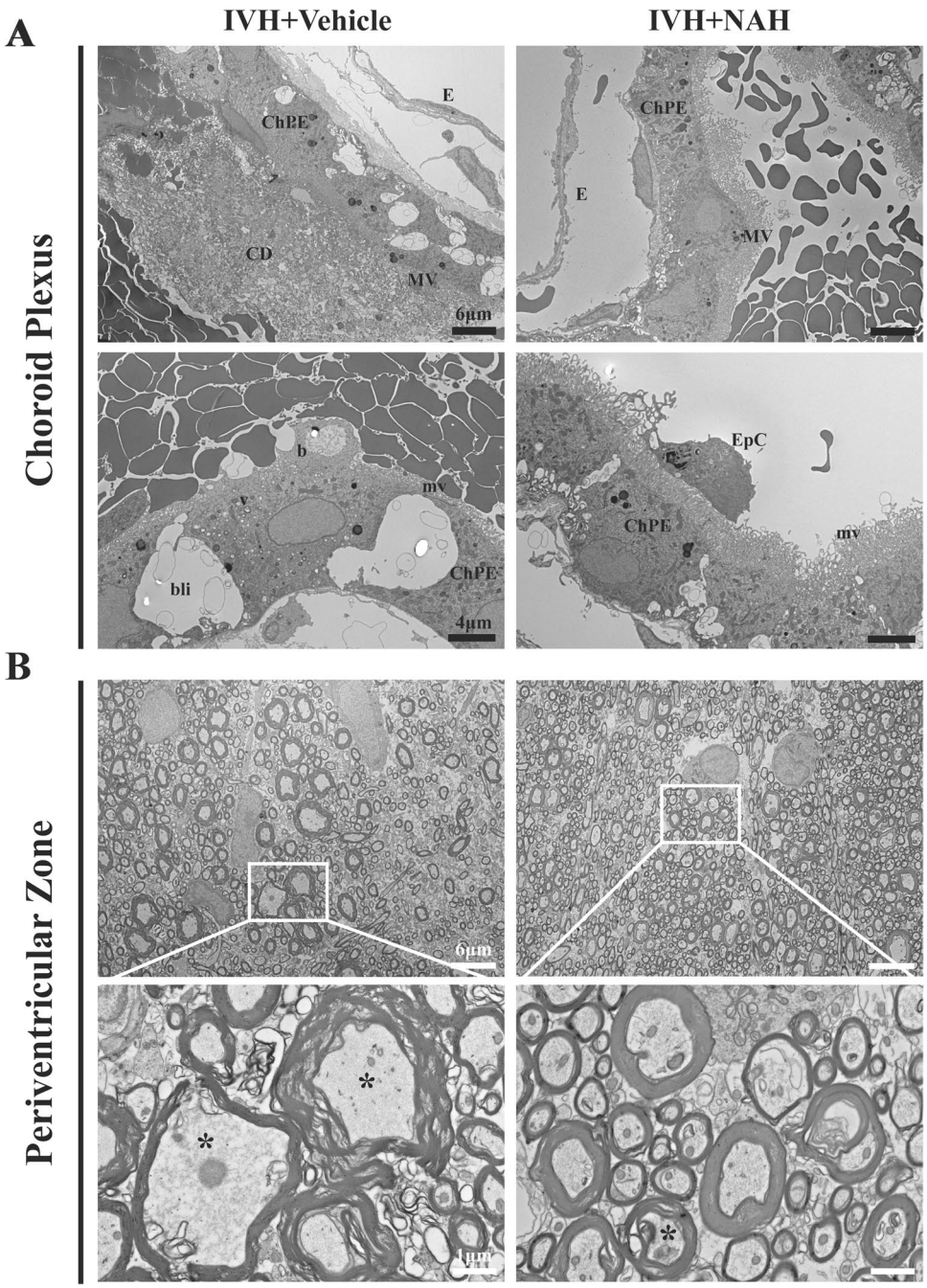

Fig. 3 NAH reduced damage to choroid plexus (ChP) and periventricular area axons after IVH. Representative electron microscopy images of ChP and periventricular zone myelinated axons 4 h after intracerebroventricular injection of blood with NAH (IVH + NAH) or saline (IVH + Vehicle) in aged rats. **A** ChP epithelial cells showed abnormal morphology in the IVH + Vehicle group with short microvilli (mv), blebbing (b) of the apical membrane, dilated basolateral interdigitations (bli) and the appearance of cellular vacuoles (v). These effects were reduced in the IVH + NAH group. Upper panel: scale bar = 6 μm, lower panel: scale bar = 4 μm, $n = 2$ per group. EpC, epiplexus cell; E, endothelium. **B** In IVH + vehicle rats, periventricular zone axons showed evidence of myelin sheath disruption (*). That was reduced in the IVH + NAH group. Upper panel: scale bar = 6 μm; lower panel: scale bar = 1 μm, $n = 2$ per group

chronically (28d) following IVH [21, 28]. The calculation of the T2* lesion volume involved multiplying the sum of intraventricular lesions in each layer by slice thickness. The presence of T2* non-hypointense lesion suggests erythrolysis according to our previous literature [29]. The sum of iso- and hyper-intense regions in each layer inside the hematoma was calculated, and multiplied by slice thickness to obtain T2* non-hypointense lesion volumes. The T2* non-hypointense lesion as a % of total T2* lesion was determined. A blinded investigator conducted above images analysis by ImageJ software (National Institutes of Health).

Brain Histology

Animals were euthanized with 100 mg/kg pentobarbital ip and perfused with 4% paraformaldehyde in 0.1 M phosphate-buffered saline (PBS, pH = 7.4). Brains were harvested and stored in 4% paraformaldehyde for 1 day, and then immersed in 30% sucrose for 2 days at 4 °C. Samples were embedded in optimal cutting temperature compound (Thermo Fisher Scientific, Waltham, MA) and coronally sectioned on a cryostat (18 μm thickness). Hematoxylin and eosin (H&E) staining was used visualize the intraventricular lesion.

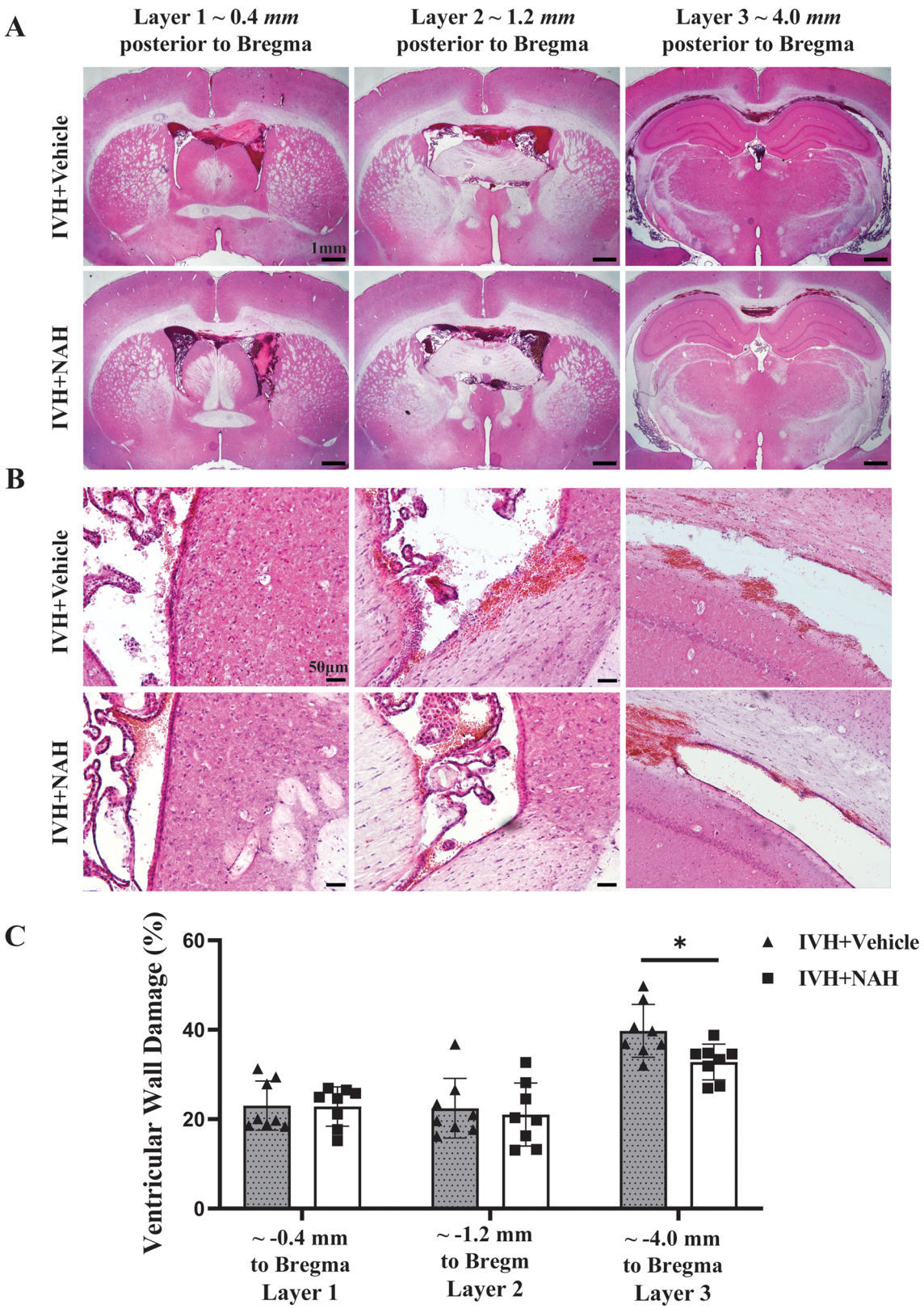
A
Layer 1 ~ 0.4 mm posterior to Bregma
Layer 2 ~ 1.2 mm posterior to Bregma
Layer 3 ~ 4.0 mm posterior to Bregma
IVH+Vehicle
IVH+NAH
1mm
B
IVH+Vehicle
IVH+NAH
50μm
C
Ventricular Wall Damage (%)
60
40
20
0
*
IVH+Vehicle
IVH+NAH
~ -0.4 mm to Bregma Layer 1
~ -1.2 mm to Bregm Layer 2
~ -4.0 mm to Bregma Layer 3

◂**Fig. 4** NAH treatment reduced ventricle wall damage at 1 day after IVH. **A** Brain hematoxylin & eosin staining at three different layers of the ventricular system one day after intracerebroventricular injection of blood with NAH (IVH + NAH) or saline (IVH + Vehicle) in aged rats. Scale bar = 1 mm. **B** Higher magnification images of ventricular wall disruption in IVH + vehicle and ICH + NAH groups. Scale bar = 50 μm. **C** Quantification of ventricular wall damage as a % of total wall length (bar graph). NAH reduced damage in layer 3 one day post-IVH. Values are shown as mean ± SD; $n = 8$ per group. *$p < 0.05$

Ventricle Wall Damage Assessment

Ventricle wall damage was assessed as described previously [30]. H&E-stained brain sections from three different layer (~ 0.4/1.2/4.0 mm posterior to bregma) were examined. Damaged ventricular wall was identified as detachment or disruption of the ependyma from the periventricular area. The percentage of ventricular wall damage was calculated by length of the overall bilateral ventricle wall surface/ damaged ventricle wall length × 100%.

Immunohistochemistry and Immunofluorescence Staining

Immunohistochemistry and immunofluorescence studies followed previous protocols [22, 31]. Primary antibodies were goat anti-complement component C3d (1:200 dilution; R&D Systems, AF2655), rabbit anti-heme oxygenase-1 (HO-1, 1:400 dilution; ADI-SPA-895-F, Enzo, New York, NY), and rabbit anti-Iba1 (1:400 dilution; Abcam, ab178846). Primary antibody omission served as a negative control. Secondary antibodies were rabbit anti-goat (1:500 dilution, Invitrogen), goat anti-rabbit (1:500 dilution, Invitrogen, Eugene, OR), and Alexa Fluor 488 donkey anti-rabbit IgG (H + L) (1:500 dilution; Invitrogen). Nuclei were labeled with hematoxylin for immunohistochemistry and 4′, 6-diamidino-2-phenylindole (DAPI; Sigma-Aldrich, St. Louis, MO) for immunofluorescence studies.

Cell Counting

Immuno-positive cells were quantified under high-power images (× 40 magnification). For periventricular cell counting, four high-power images were captured from periventricular region of each animal using a digital camera. In addition, counts of choroid plexus (ChP) cells were conducted on ipsilateral ChPs from brain sections (~ 0.4 mm posterior to bregma). Counts were normalized by calculating the number of positive cells as a percentage of all ChP cells determined using DAPI staining or H&E staining. Measurements were repeated in triplicate by a blinded observer, and the mean value used for further analysis.

Western Blotting

Western blotting was performed using previous methods [31]. In brief, periventricular brain tissue (~ 1 mm thickness) was sampled and sonicated in sample buffer. The protein content in each sample was standardized using a Bio-Rad protein assay kit. Subsequently, samples were separated using sodium dodecyl sulfate–polyacrylamide gel electrophoresis and transferred to a Hybond-C pure nitrocellulose membrane (Amersham, Pittsburgh, USA). Primary antibodies were to complement component C3d (1:2000 dilution; R&D Systems, AF2655) and hemoglobin α chain (1:1000 dilution; Abcam, ab92492). Antigen–antibody complexes were visualized using an enhanced chemiluminescence system (ECL; Amersham) and Kodak X-OMAT film. Images were analyzed using Image J software.

Electron Microscopy

Under anesthesia, rats underwent trans-cardiac perfusion with 0.1 mol/L Sorensen's buffer (pH 7.4) containing 4% paraformaldehyde and 2.5% glutaraldehyde. After harvesting the brain, coronal slices (1 mm thickness) were cut using a blade from approximately 4 mm of the frontal pole. Collected samples were submerged overnight at 4 °C in the same fixative, post-fixed with 1.0% OsO4, and dehydrated in graded ethanol. After complete dehydration, samples were infiltrated with propylene oxide and embedded in Epon. Ultra-thin sections were cut and stained with uranyl acetate and Reynold's lead citrate. Philips CM 100 transmission electron microscope was used to observe slices.

Statistical Analysis

GraphPad Prism 8 was utilized to conduct statistical analyses and generate all graphs. Unpaired student t-test was done to determine statistical significance between two groups. For comparisons involving more than two groups, one-way ANOVA was performed, followed by Tukey's multiple comparison test. Differences were considered statistically significant if the P value was < 0.05. Data are presented as means ± SD; * indicates $P < 0.05$, and ** $P < 0.01$.

Results

NAH Treatment Attenuated Complement Activation and Ventricular Dilation in the Acute Phase after IVH

Complement C3d is an indicator of complement cascade activation after hemorrhagic stroke [32]. After IVH, C3d positive cells were found at 4 h on immunohistochemistry

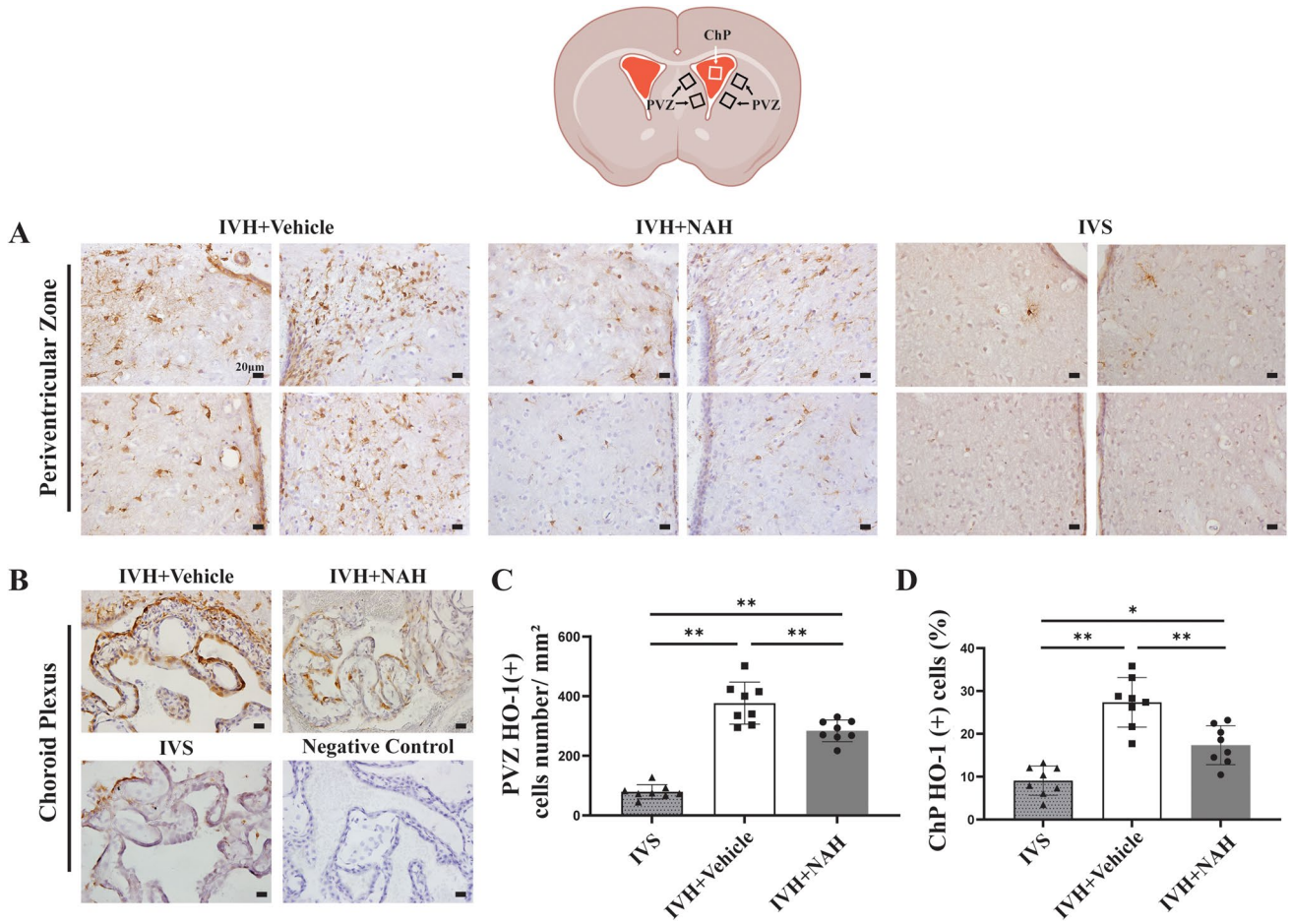

Fig. 5 NAH reduced HO-1 immunoreactivity in choroid plexus and periventricular zone one day after IVH. **A** Schematic of areas sampled for heme oxygenase (HO-1) immunohistochemistry and representative images of HO-1 positive cells in periventricular zone (PVZ) one day after intracerebroventricular blood injection with NAH (IVH + NAH), blood with saline (IVH + vehicle), or saline alone (IVS) in aged rats. Scale bar is 20 μm. **B** Representative images of choroid plexus (ChP) HO-1 positive cells. Scale bar = 20 μm. **C** Quantification of HO-1 positive cells in the PVZ one day after injection in the three groups. Note the increased number of HO-1 positive cells in both IVH + NAH and IVH + vehicle groups compared to IVS group, but that the number was reduced in the IVH + NAH group compared to the IVH + vehicle. Values are means ± SD; $n = 8$ per group. $^{**}p < 0.01$. **D** Quantification of the percentage all ChP cells that were HO-1 positive 1 day after injection in the three groups. The percentage of HO-1 positive cells increased in the IVH + vehicle group compared to the IVS group. However, the HO-1 percentage was significantly decreased in the IVH + NAH compared to the IVH + vehicle group. Values are means ± SD; $n = 8$ per group. $^{**}p < 0.01$

(Fig. 1A). On Western blot, the levels of complement C3d was significantly increased in the periventricular area after IVH (Fig. 1B; Supplemental Fig. 1) and NAH treatment significantly decreased complement C3d compared with vehicle group after 4 h of IVH (C3d/β-actin 1.23 ± 0.18 vs. 0.61 ± 0.31, $p < 0.01$). As NAH was given with the IVH, there are potential concerns over how long complement inhibition will persist. However, NAH continued to inhibit perihematomal C3d expression at 1 day as evinced on immunohistochemistry (Supplementary Fig. 2).

Ventricular volume was calculated by serial T2-weighted MRI scans (Fig. 1C). Intraventricular hemorrhage caused a significant ventricular dilation compared with IVS group on 4 h ($p < 0.01$) and 1 day ($p < 0.01$) (Fig. 1D). Co-injection of NAH significantly reduced ventricular volume compared to vehicle group both at 4 h (58.8 ± 10.0 vs. 45.4 ± 7.61 mm^3, $p < 0.01$) and 1 day (56.8 ± 10.4 vs. 42.6 ± 6.7 mm^3, $p < 0.01$).

NAH Administration Did Not Significantly Affect Hematoma Size but Attenuated Erythrolysis in the Acute Phase after IVH

Hemoglobin subunit α (HBA) is one of the byproducts of erythrolysis. Western blot analysis revealed a notable

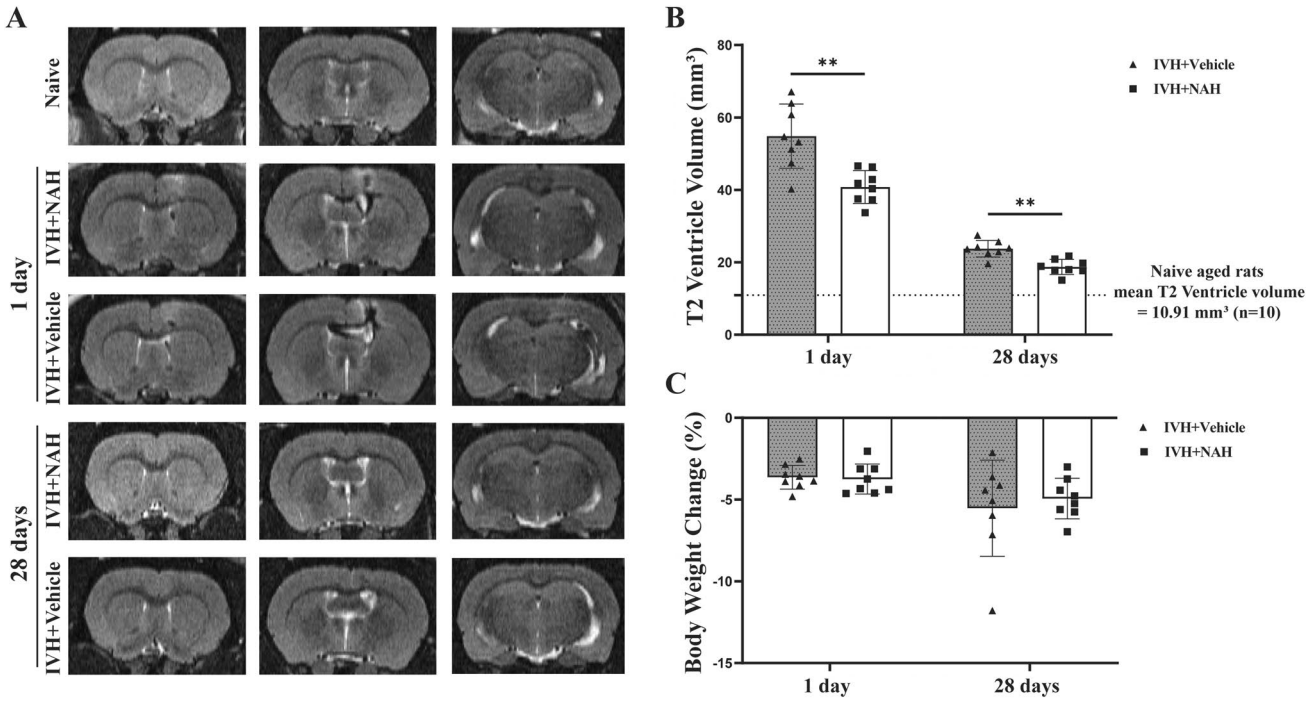

Fig. 6 NAH reduced ventricular volume in the chronic phase after IVH. **A** Representative T2-weighted MRI images 1 and 28 days after intracerebroventricular injection of blood with NAH (IVH + NAH), blood with saline (IVH + vehicle) and naïve aged F344 rats. **B** Ventricular volumes from T2-weighted images. NAH significantly reduced ventricular volume 1 day and 28 days after IVH as compared to vehicle treatment. Data are means ± SD; $n = 8$ per group, $^{**}p < 0.01$. **C** Percentage change in body weight 1 and 28 days after IVH (compared to pre-IVH weight). There were no significant differences in body weight changes between IVH + NAH and IVH + Vehicle groups

increase in periventricular HBA ($p < 0.001$) at 4 h in IVH group compared with IVS group, while NAH treatment dramatically decreased the level of HBA (0.55 ± 0.03 vs. 0.11 ± 0.10, $p < 0.001$, Fig. 2A; Supplemental Fig. 3).

Serial T2* weighted MRI scans evaluated intraventricular hematoma size and erythrolysis at 4 h and 1 day after IVH (Fig. 2B). T2* lesion volume was not significantly different between NAH and vehicle treated groups at 4 h (53.8 ± 8.0 vs. 47.8 ± 8.6 mm^3, $p = 0.17$) and 1 day (38.3 ± 10.1 vs. 32.1 ± 7.2 mm^3, $p = 0.18$, Fig. 2C). Isointense or hyperintense signal (non-hypointense signal) in the hematoma core were observed on both 4 h and 1 day after IVH. Recent studies have demonstrated that the T2* non-hypointense lesion represents the erythrolysis area in IVH model [33]. The ratio of non-hypointense T2* lesion to T2* lesion volume was calculated. The results indicated that the proportion of erythrolysis was significantly reduced in NAH group compared with vehicle group at both 4 h (8.2 ± 3.3 vs. $15.9 \pm 9.2\%$, $p < 0.05$) and 1 day (15.4 ± 5.1 vs $25.8 \pm 6.9\%$, $p < 0.01$, Fig. 2D). On electron microscopy after 4 h of IVH, NAH treatment reduced evidence of erythrocyte lysis compared to vehicle group (Fig. 2E).

NAH Treatment Alleviated Periventricular Zone and Choroid Plexus Injury in the Acute Phase After IVH

Pathological changes in the choroid plexus (ChP) epithelium were observed under electron microscopy 4 h in the IVH group treated with vehicle, with short microvilli, abnormal blebbing on the apical membrane, cellular vacuoles, dilated basolateral interdigitations and sometimes cellular debris on the apical surface (Fig. 3A). In the IVH rats treated with NAH, the ChP epithelium appeared more normal with a well-defined apical brush border (Fig. 3A). Periventricular axons in IVH rats treated with vehicle often showed disruption of the myelin sheath (Fig. 3B). This was reduced in the IVH animals treated with NAH (Fig. 3B).

To compare ependymal cell damage in NAH and vehicle treated groups one day after IVH, H&E-staining was used to analyze ventricular wall damage (Fig. 4A). Three different levels of lateral ventricular were examined, including anterior lateral ventricle (~ 0.4 mm posterior to bregma, layer 1), connection of lateral ventricle and third ventricle (~ 1.2 mm posterior to bregma, layer 2), and posterior part

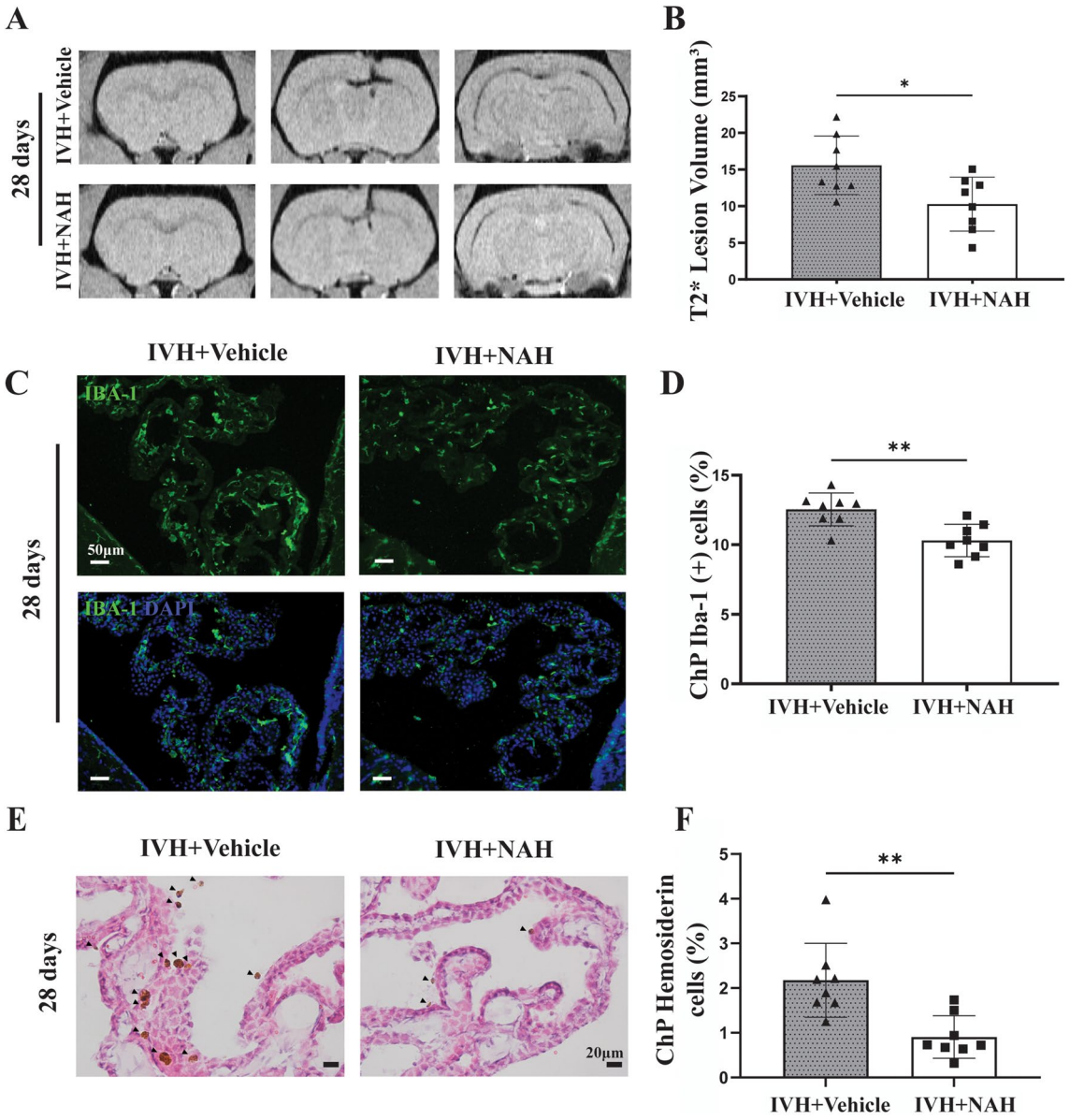

Fig. 7 NAH reduced iron deposition in the chronic phase after IVH. **A** Representative T2*-weighted MRI scans 28 days after intraventricular injection of blood with NAH (IVH + NAH) or saline (IVH + vehicle) in F344 aged rats. **B** Quantifications of T2* lesions. T2* lesions were smaller in the IVH + NAH group compared with the IVH + vehicle group. Values are means ± SD; $n = 8$ in each group, * $p < 0.05$. **C** Immunofluorescence Iba-1 staining in choroid plexus (ChP) with and without DAPI staining at 28 days after injection in the two groups. **D** Quantification of the number of Iba-1 positive cells in ChP as a percentage of all cells (DAPI). Values are means ± SD; $n = 8$ in each group, ** $p < 0.01$ between IVH + Vehicle and IVH + NAH. **E** Hematoxylin & Eosin staining of the ChP 28 days after IVH + Vehicle and IVH + NAH. Sporadic hemosiderin cells (brown) were found in the ChP. **F** Quantification of the number of hemosiderin positive cells in ChP expressed as a percentage of all cells. Values are means ± SD; $n = 8$ per group, ** $p < 0.01$ between IVH + vehicle and IVH + NAH groups

of lateral ventricle (~ 4.0 mm posterior to bregma, layer 3). Quantification of ventricular wall damage found no significant difference between vehicle and NAH groups in layer 1 (23.0 ± 5.5 vs. 22.8 ± 4.4%, $p = 0.943$) and layer 2 (22.4 ± 6.7 vs. 21.0 ± 7.1%, $p = 0.687$, Fig. 4C), but NAH treatment significantly decreased ventricular wall damage in layer 3 (39.7 ± 5.9 vs. 32.8 ± 4.0%, $p < 0.05$).

To further investigate damage to the ventricular wall and ChP, HO-1 expression in the periventricular zone (Fig. 5A) and ChP (Fig. 5B) was analyzed at 1 day after IVH. Compared with IVS group, periventricular cells positive for HO-1 and the proportion of HO-1 positive cells in the ChP were significantly up-regulated at 1 day after hemorrhage in vehicle group ($p < 0.01$). However,

compared to vehicle treatment, NAH significantly reduced the number of HO-1 positive cells in the periventricular zone (377 ± 71 vs. 284 ± 37 cells/mm^3, $p < 0.01$, Fig. 5C) as well as the proportion of HO-1 positive cells in the ChP (27.4 ± 5.8 vs. 17.4 ± 4.5% of all ChP cells, $p < 0.01$, Fig. 5D) after 1 day of IVH.

NAH Treatment Reduced the Ventricular Volume in the Chronic Phase after IVH

To assess the effects of NAH treatment on IVH-induced ventricular dilation in the chronic phase after IVH, rats underwent T2 weighted MRI (Fig. 6A). Ventricular volume was still larger than in normal aged rats at 28 days after IVH (Fig. 6B). Compared to vehicle, co-injection of NAH resulted in significantly smaller ventricular volumes at day 1 (54.8 ± 8.9 vs. 40.8 ± 4.5 mm^3, $p < 0.01$) and day 28 (23.8 ± 2.3 vs. 18.7 ± 2.1 mm^3, $p < 0.01$) after IVH. Body weight in NAH and vehicle groups were not significantly different at 1 and 28 days after operation (Fig. 6C).

NAH Treatment Reduced Iron Deposition and Choroid Plexus Iba-1 Positive Cells in the Chronic Phase after IVH

To further investigate the effects of NAH on iron deposition, T2* weighted MRI was performed 28 days after IVH (Fig. 7A). Compared to vehicle treatment, NAH-treated rats had significantly less iron deposition (15.6 ± 4.0 vs. 10.3 ± 3.7 mm^3, $p < 0.05$, Fig. 7B). In addition, Iba-1 and H&E staining were used to assess chronic changes in ChP cellular components. Compared to vehicle, NAH treatment reduced the number of Iba1-positive cells in the ChP, expressed as a % of all ChP cells (12.5 ± 1.2 vs. 10.3 ± 1.2%, $p < 0.01$, Fig. 7D). Also, compared to vehicle, the number of hemosiderin cells with NAH treatment was less than the vehicle group (2.2 ± 0.8 vs. 0.9 ± 0.5% of all ChP cells, $p < 0.01$, Fig. 7F).

Discussion

The major findings of this study are: (1) Increased C3d levels indicate the complement system is activated within 4 h after IVH in aged rats. (2) NAH, a complement inhibitor, reduced ventriculomegaly (acute and chronic) as well as ependymal, ChP and periventricular axonal damage after IVH. (3) An underlying mechanism maybe the reduced erythrolysis observed on MRI and electron microscopy with NAH. (4) Diminished erythrolysis may be responsible for reduced periventricular levels of hemoglobin subunit α, HO-1 and iron with NAH, as well as attenuated HO-1 (acute) and hemosiderin (chronic) levels in the ChP after IVH. (5) It is important to stress that these results are in aged rats enhancing potential clinical relevance as IVH after ICH in adults is primarily a disease of the elderly.

As a component of both innate and adaptive immunity, complement system plays a major role in the process of erythrolysis after ICH [18]. Different complement activation pathways converge on C3 cleavage and activation, ultimately resulting in MAC formation which forms a pore in erythrocyte membranes. This leads to erythrolysis and the release of hemoglobin after ICH [16, 26]. However, early complement cascade components have not been sufficiently studied in IVH models. Our previous study found MAC on erythrocyte cell membranes as early as 1 day after IVH in young adult rats [21]. In the current study, complement C3d, a segment of complement C3, was found around the clot as early as 4 h after intraventricular injection of autologous blood. The presence of C3d indicates the complement cascade has been activated [34]. These results are similar to previous ICH literature with complement C3d immunoreactivity being found around the clot after 24 h in a rat model [23]. In short, our results showed that the complement cascade has already been activated within 4 h after IVH in aged rats.

N-acetylheparin (NAH), a derivative of heparin, can inhibit complement activation but lacks heparins anticoagulant activity [35]. In a recent study of aged rats with ICH, NAH attenuated clot erythrolysis and neuronal death during the acute stage. Moreover, it decreased brain atrophy and iron accumulation in the chronic phase [26]. In the current study, co-injection of NAH with the IVH decreased acute (4 and 24 h) and chronic (28 days) ventriculomegaly. It also reduced ventricular wall, ChP and periventricular axonal damage, supporting that the complement cascade is a therapeutic target in IVH in aged rats.

An underlying mechanism of the protective effects of complement inhibition may be by reducing erythrolysis. The release of hemoglobin and iron after erythrolysis cause brain injury and acute ventricular enlargement after IVH [12]. Intracerebroventricular injection of lysed red blood cells caused significant ventricular enlargement and marked increases in HO-1 and ferritin expression within 24 h in adult rats. In addition, intraventricular hemoglobin and iron injection can both cause ventriculomegaly after 24 h in rodent models [13, 36, 37]. In the current study, both MRI and electron microscopy provide evidence of early erythrolysis after IVH in aged rats and that NAH can reduce erythrolysis. Indirect evidence for reduced erythrolysis also comes from reduced periventricular levels of both hemoglobin subunit α and HO-1. The latter enzyme degrades heme and is upregulated by hemoglobin exposure. HO-1 expression after IVH

was also reduced by NAH in the ChP, another tissue that would be exposed to erythrocyte lysate.

Hemoglobin degradation ultimately causes the release of iron which can be observed on T2* MRI. Iron deposition in chronic phase after cerebral hemorrhage is associated with PHH [38, 39]. Previous studies found that the incidence of hydrocephalus was 60% after 7 days and 70% after 28 days of intraventricular injection of $FeCl_3$. As an iron chelator, deferoxamine can decrease the concentrations of iron and dramatically reduced the rate of PHH [40]. The present study found that NAH treatment reduced iron deposition one month after IVH in aged rats. It also reduced the appearance of hemosiderin-positive cells in the ChP.

Recently, several studies have focused on the effect of complement inhibition on reducing secondary brain injury and PHH after IVH. Alshareef et al. injected collagenase into the subventricular zone to induce a neonatal murine GMH-IVH model. They found that CR2-Crry, a complement C3 inhibitor, reduced MAC deposition, and alleviated astrocytosis and PHH in the chronic phase after GMH-IVH [19]. In addition, Tang et al. investigated the effect of a C3a receptor antagonist in collagenase-induced GMH-IVH rats on postnatal day 7 [20]. Compared with the vehicle group, hydrocephalus and neurological function were improved with the C3a receptor antagonist. Those studies support the complement cascade as a potential therapeutic target for PHH although there are concerns that collagenase-induced brain atrophy might also result in ventriculomegaly rather than just the hematoma. An autologous blood injection model can address this concern and in our recent study, aurin tricarboxylic acid, a MAC inhibitor, was able to reduce erythrolysis and attenuate ventricular volume acutely as well as reducing iron deposition, improving PHH and functional outcome after one month in an adult rat IVH model [21]. However, that study was in young adult rats with IVH. The current study expands that to aged rats and uses another complement inhibitor. Overall, all these studies indicate that complement inhibition is a promising therapeutic target to reduce secondary brain injury after IVH including PHH.

There are several limitations of this study. First, while it provides evidence that complement inhibition can attenuate secondary brain injury after IVH, the NAH was co-injected with the blood into the lateral ventricle, which limits clinical relevance. Repeated intracerebroventricular injections (for IVH and drug administration) in a small species such as rat poses significant issues. Direct CSF administration is feasible in human IVH as an external ventricular drainage (EVD) combined with rt-PA administration is a common clinical management decision for IVH patients with obstructive hydrocephalus [5]. Future studies should explore the effects of delayed injection of NAH after an EVD. An alternative is the development of blood–brain barrier permeable complement inhibitors. Second, this study only used male F344 aged rats. The effects of complement inhibition should be examined in female rodents. Third, further studies are needed to extrapolate these results to neonatal GMH-IVH.

In conclusion, the complement cascade is an attractive target for limiting IVH-induced brain injury and PHH. Our results indicate it remains a target even in aged animals.

Supplementary Information The online version contains supplementary material available at https://doi.org/10.1007/s12975-024-01273-6.

Author Contributions TZ, FX, and YW performed animal experiments. TZ and FX contributed to data analysis. TZ wrote the manuscript. YH, RFK, and GX conceived the initial research plan and supervised the project. All the authors read, edited and approved the final manuscript.

Funding Y.H., R.F.K. and G.X. were supported by grants NS-106746 and NS-116786 the National Institutes of Health.

Data Availability All data supporting the findings of this study are available within the paper.

Declarations

Ethical Approval The animal research in this article adheres to ethical guidelines. The animal use protocols were approved by the Committee on the Use and Care of Animals of the University of Michigan (PRO00009619 and PRO00011197).

Competing Interests The authors declare no competing interests.

References

1. Trifan G, Arshi B, Testai FD. Intraventricular hemorrhage severity as a predictor of outcome in intracerebral hemorrhage. Front Neurol. 2019;10:217. https://doi.org/10.3389/fneur.2019.00217.
2. Bhattathiri PS, Gregson B, Prasad KS, Mendelow AD. Intraventricular hemorrhage and hydrocephalus after spontaneous intracerebral hemorrhage: results from the STICH trial. Acta Neurochir Suppl. 2006;96:65–8. https://doi.org/10.1007/3-211-30714-1_16.
3. Balami JS, Buchan AM. Complications of intracerebral haemorrhage. Lancet Neurol. 2012;11(1):101–18. https://doi.org/10.1016/s1474-4422(11)70264-2.
4. Christian EA, Jin DL, Attenello F, Wen T, Cen S, Mack WJ, Krieger MD, McComb JG. Trends in hospitalization of preterm infants with intraventricular hemorrhage and hydrocephalus in the United States, 2000–2010. J Neurosurg Pediatr. 2016;17(3):260–9. https://doi.org/10.3171/2015.7.Peds15140.
5. Greenberg SM, Ziai WC, Cordonnier C, Dowlatshahi D, Francis B, Goldstein JN, Hemphill JC 3rd, Johnson R, Keigher KM, Mack WJ, et al. 2022 guideline for the management of patients with spontaneous intracerebral hemorrhage: a guideline from the American Heart Association/American Stroke Association. Stroke. 2022;53(7):e282–361. https://doi.org/10.1161/str.0000000000000407.
6. Steiner T, Diringer MN, Schneider D, Mayer SA, Begtrup K, Broderick J, Skolnick BE, Davis SM. Dynamics of intraventricular hemorrhage in patients with spontaneous intracerebral hemorrhage: risk factors, clinical impact, and effect of hemostatic

therapy with recombinant activated factor VII. Neurosurgery. 2006;59(4):767–773; discussion 773–764. https://doi.org/10.1227/01.Neu.0000232837.34992.32.
7. Caldarelli M, Di Rocco C, La Marca F. Shunt complications in the first postoperative year in children with meningomyelocele. Child's Nerv Syst. 1996;12(12):748–54. https://doi.org/10.1007/bf00261592.
8. Riva-Cambrin J, Kestle JR, Holubkov R, Butler J, Kulkarni AV, Drake J, Whitehead WE, Wellons JC 3rd, Shannon CN, Tamber MS, et al. Risk factors for shunt malfunction in pediatric hydrocephalus: a multicenter prospective cohort study. J Neurosurg Pediatr. 2016;17(4):382–90. https://doi.org/10.3171/2015.6.Peds14670.
9. Wong T, Gold J, Houser R, Herschman Y, Jani R, Goldstein I. Ventriculopleural shunt: Review of literature and novel ways to improve ventriculopleural shunt tolerance. J Neurol Sci. 2021;428: 117564. https://doi.org/10.1016/j.jns.2021.117564.
10. Ertuğrul B, Kaplan M, Batu Hergünsel Ö, Akgün B, Öztürk S, SerhatErol F. The effectiveness of antibiotic-coated ventriculoperitoneal shunts for prevention of shunt infections in patients with myelomeningocele. Pediatr Neurosurg. 2021;56(4):357–60. https://doi.org/10.1159/000516379.
11. Mitchell KS, Zelko I, Shay T, Horen S, Williams A, Luciano M, Huang J, Brem H, Gordon CR. The impact of hydrocephalus shunt devices on quality of life. J Craniofac Surg. 2021;32(5):1746–50. https://doi.org/10.1097/scs.0000000000007579.
12. Holste KG, Xia F, Ye F, Keep RF, Xi G. Mechanisms of neuroinflammation in hydrocephalus after intraventricular hemorrhage: a review. Fluids Barriers CNS. 2022;19(1):28. https://doi.org/10.1186/s12987-022-00324-0.
13. Gao C, Du H, Hua Y, Keep RF, Strahle J, Xi G. Role of red blood cell lysis and iron in hydrocephalus after intraventricular hemorrhage. J Cereb Blood Flow Metab. 2014;34(6):1070–5. https://doi.org/10.1038/jcbfm.2014.56.
14. Chen Z, Gao C, Hua Y, Keep RF, Muraszko K, Xi G. Role of iron in brain injury after intraventricular hemorrhage. Stroke. 2011;42(2):465–70. https://doi.org/10.1161/strokeaha.110.602755.
15. Chen Q, Tang J, Tan L, Guo J, Tao Y, Li L, Chen Y, Liu X, Zhang JH, Chen Z, et al. Intracerebral hematoma contributes to hydrocephalus after intraventricular hemorrhage via aggravating iron accumulation. Stroke. 2015;46(10):2902–8. https://doi.org/10.1161/strokeaha.115.009713.
16. Cao S, Zheng M, Hua Y, Chen G, Keep RF, Xi G. Hematoma changes during clot resolution after experimental intracerebral hemorrhage. Stroke. 2016;47(6):1626–31. https://doi.org/10.1161/strokeaha.116.013146.
17. Wang M, Xia F, Wan S, Hua Y, Keep RF, Xi G. Role of complement component 3 in early erythrolysis in the hematoma after experimental intracerebral hemorrhage. Stroke. 2021;52(8):2649–60. https://doi.org/10.1161/strokeaha.121.034372.
18. Holste K, Xia F, Garton HJL, Wan S, Hua Y, Keep RF, Xi G. The role of complement in brain injury following intracerebral hemorrhage: A review. Exp Neurol. 2021;340: 113654. https://doi.org/10.1016/j.expneurol.2021.113654.
19. Alshareef M, Hatchell D, Vasas T, Mallah K, Shingala A, Cutrone J, Alawieh A, Guo C, Tomlinson S, Eskandari R. Complement drives chronic inflammation and progressive hydrocephalus in murine neonatal germinal matrix hemorrhage. Int J Mol Sci. 2023;24(12):10171. https://doi.org/10.3390/ijms241210171.
20. Tang J, Jila S, Luo T, Zhang B, Miao H, Feng H, Chen Z, Zhu G. C3/C3aR inhibition alleviates GMH-IVH-induced hydrocephalus by preventing microglia-astrocyte interactions in neonatal rats. Neuropharmacology. 2022;205: 108927. https://doi.org/10.1016/j.neuropharm.2021.108927.
21. Holste KG, Ye F, Koduri S, Garton HJL, Maher CO, Keep RF, Hua Y, Xi G. Attenuation of ventriculomegaly and iron overload after intraventricular hemorrhage by membrane attack complex inhibition. J Neurosurg. 2023:1–11. https://doi.org/10.3171/2023.8.Jns23667.
22. Wan Y, Gao F, Ye F, Yang W, Hua Y, Keep RF, Xi G. Effects of aging on hydrocephalus after intraventricular hemorrhage. Fluids Barriers CNS. 2020;17(1):8. https://doi.org/10.1186/s12987-020-0169-y.
23. Hua Y, Xi G, Keep RF, Hoff JT. Complement activation in the brain after experimental intracerebral hemorrhage. J Neurosurg. 2000;92(6):1016–22. https://doi.org/10.3171/jns.2000.92.6.1016.
24. Park JL, Kilgore KS, Naylor KB, Booth EA, Murphy KL, Lucchesi BR. N-Acetylheparin pretreatment reduces infarct size in the rabbit. Pharmacology. 1999;58(3):120–31. https://doi.org/10.1159/000028274.
25. Nakamura T, Vollmar B, Winning J, Ueda M, Menger MD, Schäfers HJ. Heparin and the nonanticoagulant N-acetyl heparin attenuate capillary no-reflow after normothermic ischemia of the lung. Ann Thorac Surg. 2001;72(4):1183–1188; discussion 1188–1189. https://doi.org/10.1016/s0003-4975(01)02959-9.
26. Wang M, Hua Y, Keep RF, Wan S, Novakovic N, Xi G. Complement inhibition attenuates early erythrolysis in the hematoma and brain injury in aged rats. Stroke. 2019;50(7):1859–68. https://doi.org/10.1161/strokeaha.119.025170.
27. Percie du Sert N, Hurst V, Ahluwalia A, Alam S, Avey MT, Baker M, Browne WJ, Clark A, Cuthill IC, Dirnagl U, et al. The ARRIVE guidelines 2.0: Updated guidelines for reporting animal research. PLoS Biol. 2020;18(7):e3000410. https://doi.org/10.1371/journal.pbio.3000410.
28. Wu G, Xi G, Hua Y, Sagher O. T2* magnetic resonance imaging sequences reflect brain tissue iron deposition following intracerebral hemorrhage. Transl Stroke Res. 2010;1(1):31–4. https://doi.org/10.1007/s12975-009-0008-6.
29. Dang G, Yang Y, Wu G, Hua Y, Keep RF, Xi G. Early erythrolysis in the hematoma after experimental intracerebral hemorrhage. Transl Stroke Res. 2017;8(2):174–82. https://doi.org/10.1007/s12975-016-0505-3.
30. Okubo S, Strahle J, Keep RF, Hua Y, Xi G. Subarachnoid hemorrhage-induced hydrocephalus in rats. Stroke. 2013;44(2):547–50. https://doi.org/10.1161/strokeaha.112.662312.
31. Xi G, Keep RF, Hua Y, Xiang J, Hoff JT. Attenuation of thrombin-induced brain edema by cerebral thrombin preconditioning. Stroke. 1999;30(6):1247–55. https://doi.org/10.1161/01.str.30.6.1247.
32. Xi G, Hua Y, Keep RF, Younger JG, Hoff JT. Systemic complement depletion diminishes perihematomal brain edema in rats. Stroke. 2001;32(1):162–7. https://doi.org/10.1161/01.str.32.1.162.
33. Ye F, Hua Y, Keep RF, Xi G, Garton HJL. CD47 blocking antibody accelerates hematoma clearance and alleviates hydrocephalus after experimental intraventricular hemorrhage. Neurobiol Dis. 2021;155: 105384. https://doi.org/10.1016/j.nbd.2021.105384.
34. Bellander BM, von Holst H, Fredman P, Svensson M. Activation of the complement cascade and increase of clusterin in the brain following a cortical contusion in the adult rat. J Neurosurg. 1996;85(3):468–75. https://doi.org/10.3171/jns.1996.85.3.0468.
35. Weiler JM, Edens RE, Linhardt RJ, Kapelanski DP. Heparin and modified heparin inhibit complement activation in vivo. J Immunol. 1992;148(10):3210–5.
36. Shishido H, Toyota Y, Hua Y, Keep RF, Xi G. Role of lipocalin 2 in intraventricular haemoglobin-induced brain injury.

Stroke Vasc Neurol. 2016;1(2):37–43. https://doi.org/10.1136/svn-2016-000009.
37. Strahle JM, Garton T, Bazzi AA, Kilaru H, Garton HJ, Maher CO, Muraszko KM, Keep RF, Xi G. Role of hemoglobin and iron in hydrocephalus after neonatal intraventricular hemorrhage. Neurosurgery. 2014;75(6):696–705; discussion 706. https://doi.org/10.1227/neu.0000000000000524.
38. Pan S, Hale AT, Lemieux ME, Raval DK, Garton TP, Sadler B, Mahaney KB, Strahle JM. Iron homeostasis and post-hemorrhagic hydrocephalus: a review. Front Neurol. 2023;14:1287559. https://doi.org/10.3389/fneur.2023.1287559.
39. Iwanowski L, Olszewski J. The effects of subarachnoid injections of iron-containing substances on the central nervous system. J Neuropathol Exp Neurol. 1960;19:433–48. https://doi.org/10.1097/00005072-196007000-00010.
40. Meng H, Li F, Hu R, Yuan Y, Gong G, Hu S, Feng H. Deferoxamine alleviates chronic hydrocephalus after intraventricular hemorrhage through iron chelation and Wnt1/Wnt3a inhibition. Brain Res. 2015;1602:44–52. https://doi.org/10.1016/j.brainres.2014.08.039.